Effect of Pre-treatment Conditions on the Electrochemical Performance of Bio-waste Derived Carbon.

Mutiat Modupe Oniye, B.Eng.

Submitted in fulfilment of the requirements for the degree of Master of Science in Chemical & Material Engineering

School of Engineering and Digital Sciences

Department of Chemical and Materials Engineering

Nazarbayev University

53 Kabanbay Batyr Avenue,

Astana, Kazakhstan, 010000

Supervisor: Dr. Aishuak Konarov

Co-supervisor: Dr. Fail Sultanov

April, 2024

Declaration

I hereby, declare that this manuscript, entitled “Effect of Pre-treatment Conditions on the Electrochemical Performance of Bio-waste Derived Carbon”, is the result of my work except for quotations and citations which have been duly acknowledged.

I also declare that, to the best of my knowledge and belief, it has not been previously or concurrently submitted, in whole or in part, for any other degree or diploma at Nazarbayev University or any other national or international institution.

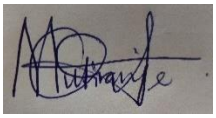

Name: Mutiat Modupe Oniye

Date: 02.05.2024

Abstract

Energy companies like CATL, SVOLT, Tiamat, and Natron are actively working on commercializing Sodium-ion Batteries. These batteries offer advantages over Lithium-ion batteries, due to even sodium distribution, relatively inexpensive electrode materials, and safer transportation. The synthesis of Hard-Carbons as anode material is a promising avenue for developing high-capacity Sodium-ion Batteries, given their low insertion voltage and wide interlayer spacing, which enhances sodium-ion insertion. While traditionally these Hard-Carbons are derived from costly carbonaceous materials, the use of abundantly available carbonaceous bio-waste like coffee-waste as Hard-Carbon precursors would not only lower production costs but also contribute to global waste management and disposal.

However, the electrochemical performance of bio-waste-derived Hard-Carbon is significantly affected by pre-treatment conditions, both before and after thermal treatment. This research employed characterization techniques like XRD, TEM, and SEM to investigate the impact of pre-treatment conditions, such as washing with various solvents (organic solvent, acid, or distilled water), pre-oxidation and pre-pyrolysis on the coffee-waste-derived hard carbon structure and purity, which consequently influence the electrochemical capacity of the synthesized negative electrode for Sodium-ion Batteries.

A 23% yield mesoporous hard-carbon synthesized from washing coffee grounds with de-ionized water and pre-oxidation at 150℃ before thermal treatment at 1300℃ using 5℃/min ramping rate in an argon environment demonstrated an excellent deliverable capacity of 304mAhg^{-1} and an Initial Coulombic Efficiency of 78%. This study highlights how the washing solvent and pre-oxidation improved the electrochemical performance due to the presence of inorganic impurities and expansion of the graphite inter-layer distance which improves the carbon-oxygen composition, electronic conductivity and sodium insertion of the electrode.

Acknowledgement

Firstly, I would like to express my uttermost gratitude to my supervisors Dr. Konarov and Dr. Sultanov. It has been their supervision and direction throughout the research period which has allowed me to complete this Master's program. I appreciate all the hours of discussion they have offered me, especially in characterization and result discussions.

Secondly, I would like to show my indebtedness to the provost staff of Nazarbayev University, especially at the Core Facilities Laboratory whose efforts often go unnoticed for their kind support and assistance during this program.

This research is part of the research project supported by the Ministry of Education and Science of the Republic of Kazakhstan Grant (AP09259165), "Utilization of the biowaste-derived carbon and enhancement of its electrochemical performance via doping".

Finally, I would like to thank my partner, family, colleagues and friends who provided me with the necessary support to complete this program.

Table Of Contents

List of Abbreviations & Symbols

AB	Acetylene Black
AHC	Acid-washed Hard Carbon
BHC	D.I -washed Hard Carbon
CHC	Cyclohexane-washed Hard Carbon
CGs	Coffee Grounds
DMC	Dimethyl Carbonate
EC	Ethylene Carbonate
FEC	Fluoroethylene Carbonate
HC	Hard Carbon
ICE	Initial Coulombic Efficiency
LIBs	Lithium – Ion Batteries
NMP	N – Methyl – 2 – Pyrrolidone
PVDF	Polyvinylidene Fluoride
SEI	Solid Electrolyte Interphase
SEM	Scanning Electron Microscopy
SIBs	Sodium – Ion Batteries
TEM	Transmission Electron Microscopy
XRD	X – Ray Diffraction

List of Tables And Figures

Chapter 1 – Introduction

Over the years, the rapid depletion of fossil fuel and its non-regenerative characteristics has been an issue of great concern, coupled with the significant change in climate conditions such as global warming, Green House Gases (GHG) emissions, and others as a result of fossil burning which has led to severe health and environmental issues, has compelled researchers to find an eco-friendly yet sustainable solution to fossil fuel. To find a lasting solution to sustainable and regenerative energy, the study of regenerative powers and their properties is of great importance[1].

Rechargeable batteries provide a sustainable alternative to non-regenerative fossil fuel due to their unique properties, which include storage, low toxicity, and cheap production cost; the most suitable option identified was Lithium-Ion Batteries (LIBs) as they possess good cycle life, high capacity, and energy density alongside its carrier ion lightness. Therefore, it was employed in the design of electronics such as phones and electric cars [2].

However, some issues arose over the years as Li is unevenly distributed globally and the storage mechanism is limited; this led to a massive rise in the cost of large production as raw materials became expensive due to unavailability, and LIBs failed some of the required properties large–scale energy production and storage, this prompted the search for an alternative solution to LIBs using readily available elements such as Sodium (Na) and Potassium (K) which are the 6^{th} and 7^{th} most abundant resources globally, therefore solving sustainability, market demand and cheap cost of production for rechargeable batteries [3].

These elements' ions (Na^+ & K^+) possess similar chemical properties, electronegativity, and intercalation chemistry with Lithium ions (Li^+) because these three elements belong to group IA on the periodic table, hence their potential to easily replace LIBs[4]. Owing to this similarity among the alkaline earth metals, graphite material was employed as an active electrode for Na^+ batteries (SIBs) as a result of its numerous advantages over other LIBs anode materials, such as its theoretical capacity of 372mAhg-1, high ICE (Initial Coulombic Efficiency), shallow plateau profile and excellent cycling stability [5].

However, as a result of sodium's larger ionic radius (0.102nm) compared to lithium's ionic radius (0.076nm), a low capacity of approximately 130mAhg-1 was observed when graphite was used as anode material as a result of the difficulties involved during intercalation of Na^+ into graphite layer (0.335nm) [6]. Production of sustainable anode materials with sufficient energy density, low cost of production, and good reversible capacity is of great importance in SIBs.

Some of the negative electrode materials proposed for SIBs include oxides of metals, metal phosphides, sodium alloys, and carbonaceous materials; the carbonaceous material is the only suitable material for SIBs as a result of its large interlayer spacing and random unorganized structure, although sodium alloy possesses a great capacity, it changes volume upon charge-discharge cycle which leads to poor durability and structural decomposition [7].

Stevens and Dahn's disclosure of the Na^+ insertion mechanism in Hard–Carbon (HC) in the late 20^{th} century made the required turning point in SIB development [8]. Employing Carbonaceous material such as HC as electrode material produced an excellent reversible specific capacity of approximately 300mAhg-1, which is the closest sodium capacity to the lithium capacity of 372mAhg-1; this serves as the basis for the current SIBs study[9]. This discovery led to more interest in improving Sib's overall performance; consecutively, HC keeps up with the trend. Figure 1 shows the development in HC as interest in SIBs grows.

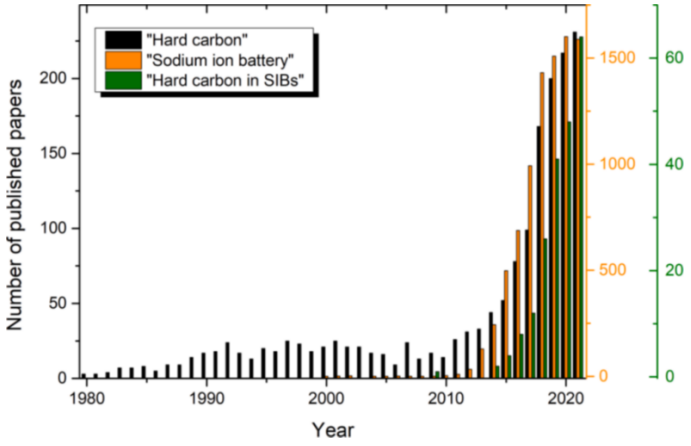

Figure 2. Chart Illustrating the Growth in HC in SIBs, SIBs, and HC [9].

HC is synthesized from biomass, as biomass is the cheapest yet eco-friendly source for carbonaceous material; utilization of biomass for HC synthesis not only solves issues of energy concern but also effectively handles biomass disposal problem[10]; furthermore, HC synthesized from biomass unique properties such as Porosity, morphology which are beneficial for transportation and storage of Na^+. Lignin and cellulose, the most abundant biopolymer, are the principal constituents responsible for carbon formation. These constituents influence the HC properties derived from the biomass, as the primary organic components of plant-based biomass are lignin, cellulose, and protein[11].

1.1 Aim

This thesis aims to investigate the effect of pre-treatment conditions such as pre-oxidation in air and pre–pyrolysis on SIBs electrochemical rate performance using HC synthesized from biowaste as active electrode material by studying Na^+ insertion and extraction mechanism in the material.

1.2 Objectives

- Sample preparation using Organic solvents, Deionized water, and Acid, to remove impurities and unwanted inorganic elements.
- Sample pre-treatment utilizing pre-oxidation, pre-pyrolysis and direct thermal treatment before HC Synthesis at a specified temperature and ramping rate to evaluate the influence of pre-treatment conditions on the electrochemical behaviour of the synthesized HC.
- Electrode Preparation and Evaluation of synthesized HC electrochemical performance employing Galvanostatic charge-discharge, Cyclic voltammetry, and others.
- Characterization of synthesized HC: phase analysis employing X-ray diffraction (XRD), determination of morphology and interparticle arrangement using Electron Microscopy, and elemental analysis through CHNS.

Chapter 2 – Literature Review

Following the discovery of sodium intercalation in HC, several studies derived HC from plant-based biomass by changing the synthesis route, operating temperature, and conditions while investigating the influence of this on the Na^+ storage mechanism and behaviors [12]. Similarly, some studies have been carried out to optimize the energy density and specific capacity of SIBs using HC as anode materials, alongside manipulation of the synthesis condition to enhance the electrochemical performance while studying the factors responsible for the decrease in electrochemical performance and the connection between the precursor for HC and storage mechanism for Sodium-Ion.

Although bio-waste derived HC demonstrated high–rate performance, the link between the precursor and derived HC electrochemical performance is yet to be confirmed. A detailed analysis of the effect of biomass properties on the HC's yield and structural composition is essential. It provides information on optimal operating conditions for precursors to achieve high HC yield alongside outstanding electrochemical performance[13]. High-performance HC has been developed over the years by optimizing two essential criteria: identifying the HC precursor with the potential to deliver high capacity and the optimal synthesis condition that supports this precursor.

Wu, et al. [13] compared the electrochemical performance of microcrystalline cellulosic HC with milled–wool Lignin HC through the characterization of HC to investigate the functional sites present and the active components while studying the lattice surface upon evaluation of the electrochemical performance, microcrystalline cellulosic HC demonstrated a higher reversible capacity with less trapping of Sodium Ion, which led to the adoption of peanut shell for further investigation of the results, as peanut possess high cellulose composition to lignin, the Biowaste-derived HC demonstrated similar behavior with the cellulosic HC producing Initial Coulombic Efficiency (ICE) of about eighty percent with a stable capacity of 312.3mAhg-1.

However, the synthesized HC Na^+ insertion mechanism and effects of the synthesis condition on Na^+ storage remain unclear; Alvin, et al. [14] conducted some studies to investigate the storage mechanism of Na^+ in HC by examining the connection between the reversible plateau and sloping region capacity gain with the active sites in the HC, employing HC synthesized from lignin where the physicochemical properties and ex–situ characterization techniques revealed the four stage storage mechanism involving defect sites adsorption, micropores filling for the sloping region, then micro – pores adsorption near the cut – off potential and interlayers insertion for the plateau region.

Furthermore, Chen, et al. [15] studied the influences of HC precursor microstructure on Na^+ storage mechanism in two different types of HC, employing Raman analysis, XRD, and other characterization techniques, it confirmed that the shallow plateau between 0.01V – 0.25V is made up of capacity gained from intercalation of Na^+ into the HC interlayer and capacity gain from the HC micro – pores filling. Precursor morphology significantly influences the capacity gain from these two storage mechanisms. Based on their discovery, the authors suggested a storage mechanism composed of HC interlayer insertion and micropores filling for HCs, termed HYBRID Na^+ STORAGE MECHANISM.

Table 2.0 Selected Studies Carried Out on SIBs using Biomass–Derived HC as Anode Materials.

S/N	Title [ref]	Anode Material	Novelty	Conclusion
1	" Impact of Biomass Inorganic Impurities on HC Properties and Performance in Na-ion Batteries " [17]	Asparagus, Grape, & Potato	Investigate the Effect of Pre/Post TT Washing on HC Performance	Washing with HCl Post TT Improves the Performance by Increasing the Microporosity from washing of Crystalline Inorganic Impurities.
2	" Coffee-ground-derived *NanoPorous* Carbon Anodes for SIBs with High-rate Performance and Cyclic Stability " [18]	Coffee-ground	Evaluation of the Relationship Between Surface Area, Pore Size, and Battery Performance alongside the influence of Activating Agent on the HC Properties.	Activating Agents Influence the Porosity, thereby Influencing the Performance through Sodium Ion Transportation. Higher Porosity is observed at Susceptor to Biomass Ratio of 5:1
3	" Impact of Pre-oxidation Treatments on Performances of Pitch-based HCs for SIBs" [19]	Pitch Precursor	Influence of Pre-oxidation period & Environment on HC behaviour and Properties.	Pre-oxidation in the oxygen Environment Increases the Storage Capacity, whereby Porosity and defects depend on the Pre-oxidation Duration.

4	" Biomass HC of High ICE for Sodium-ion Batteries: Preparation & Application " [20]	Camphor Wood Residues	Evaluation of the Major Factors Influencing the ICE	The Initial Irreversible Capacity Loss, Responsible for ICE Majorly, depends on the Defects Influenced by the Synthesis Heating Rate.
5	" Revealing the Sodium Storage Behavior of Biomass-derived HC Using Pure Lignin and Cellulose as Model Precursors " [13]	Milled-wool Lignin & Microcrystalline Cellulose	Evaluation of the Storage Mechanism to Investigate the Contribution of Each Component to the Storage Performance.	Cellulose Promotes High ICE and Reversible Capacity due to Its Low I_D/I_G Values, and this Enhances the Diffusion of Sodium Ions, Conductivity, and Large Plateau Capacity.
6	" Sulphur and phosphorus co-doped HC derived from oak seeds enabled reversible sodium spheres filling and plating for ultra-stable sodium storage " [21]	Biomass Oak seeds	Biomass Oak seeds from biomass were used as precursors for synthesizing S/P co-doped HC using a straightforward one stage pyrolysis method.	The distinctive S/P co-doping significantly contributes to enhanced electrochemical performance due to sulfur and phosphorus' abilities to increase interlayer spacing and improve thorough sodium charge transfer kinetics within the HC structure.
7	" Waste coffee grounds-derived carbon: nanoarchitecture pore-structure regulation for sustainable room-temperature sodium–sulphur batteries "[22]	Waste Coffee Grounds	This study established a strong relationship between precisely regulating carbon material pore structures and their electrochemical behaviour, showcasing a link between biowaste and efficient energy storage materials.	Tailoring carbon structures to include micro-, meso-, and macropores yields favorable properties such as improved wettability and enhanced accessibility, which are crucial for efficient performance. Optimizing carbon with an appropriate sulfur composition notably increased its capacity retaining properties and cycle stability in room temperature Na–S batteries.
8	" A Stable Biomass-Derived HC Anode for High- Performance Sodium-Ion Full Battery"[23]	Bagasse	Investigate the role of bagasse as a high surface area carbon precursor for high-stability sodium-ion batteries.	The complete battery system achieves a high mid-point voltage (2.9 V), with a remarkable ICE of 93.1%, and maintains excellent cycling and capacity

				stability with a 61% retention after 300 cycles at 125 mA/g.
9	" The novel N-rich HC nanofiber as high-performance electrode materials for sodium-ion batteries "[24]	Kitchen biowaste (eggshell)	Development of nitrogen-rich nanofiber carbon for SIBs from eggshell using a direct carbonization pathway.	Nitrogen-rich carbon nanofibers treated at 1300°C exhibit superior electrochemical performance with high capacity with good retention and stability of 301mA/g at 0.1C rate with an ICE of 80.0%.
10	" Biomass-derived N/S dual-doped porous hard-carbon as high-capacity anodes for lithium/sodium ions batteries"[25]	Medicine Residue	Development of high-capacity dual-doped anode material using medicine residue as carbon precursor.	N/S-PC material exhibits outstanding performance in both rate capability and cycling stability for LIBs and SIBs by leveraging the synergistic effects of nitrogen and sulfur double doping on increased surface area and edge defects,

Chapter 3 – Methodology

3.1 Material Synthesis

3.1.0 Collection and Preparation of Biowaste

Coffee Grounds (CGs) were collected from the Health Project coffee house (Astana, Kazakhstan). CGs collected were dried at 80℃ in a natural convection laboratory oven - PN (Carbolite Gero) for 24h for optimal moisture removal [17]. The dried CGs were then divided into 3 portions (50g each) and treated with 250ml of 3 different solvents which are cyclohexane, de-ionized water and hydrochloric acid for 12 hours using a stirrer at 100rpm for optimal removal of organic impurities and inorganic matters. This was followed by filtration using a vacuum filtration set, and the obtained CGs were dried at 80℃ overnight [26].

3.1.1 Biowaste Treatment and Hard Carbon Synthesis

The treated CGs were stored in an airtight container and labelled CG1 (Coffee-ground treated with cyclohexane), CG2 (Coffee-ground treated with de-ionized water) and CG3 (Coffee-ground treated with hydrochloric acid) for the 3 different solvents used, then three different HC samples were prepared from each treated CGs using 3 different treatment conditions which are pre-oxidation, pre-pyrolysis and direct thermal treatment. The synthesized HCs from the 3 different solvents under 3 different pre-treatment conditions were labelled as:

CHC-150°C: 10.013g of CG1 was weighed and pre-oxidized at 150°C in a muffle oven for 2 hours. The pre-oxidized CG1 was then carbonized at a thermal treatment temperature of 1300°C, using a dwelling period of 2 hours at a ramping rate of $5℃/min$ under an Argon environment in a high-temperature tube furnace (Carbolite Gero).

CHC-600°C: 10.00g of CG1 was pre-pyrolyzed for 2 hours at 600°C at $5℃/min$ ramping rate under an Argon environment in a high-temperature tube furnace. The resulting biochar was washed with deionized water for further removal of impurities, and oven-dried at 80°C for 12 hours. The resulting biochar was carbonized at a heat treatment temperature of

1300°C using a dwelling period of 2 hours at a ramping rate of 5℃/min under an Argon environment in a high-temperature tube furnace (Carbolite Gero).

CHC-1300°C: 10.0014g of CG1 was directly carbonized at a heat treatment temperature of 1300°C for 2 hours at a ramping rate of 5℃/min under an Argon environment in a high-temperature tube furnace (Carbolite Gero).

BHC-150°C: 10.0016g of CG2 was weighed and pre-oxidized at 150°C in a muffle oven for 2 hours. The pre-oxidized CG2 was then carbonized at a thermal treatment temperature of 1300°C, for 2 hours at a ramping rate of 5℃/min under an Argon environment in a high-temperature tube furnace (Carbolite Gero).

BHC-600°C: 10.0g of the dried CG2 was pre-pyrolyzed for 2 hours at 600°C at 5℃/min ramping rate under an Argon environment in a high-temperature tube furnace. The resulting biochar was washed with deionized water for further removal of impurities, and oven-dried at 80°C for 12 hours. The resulting biochar was carbonized at a heat treatment temperature of 1300°C using a dwelling period of 2 hours at a ramping rate of 5℃/min under an Argon environment in a high-temperature tube furnace (Carbolite Gero).

BHC-1300°C: 10.0g of CG2 was directly carbonized at a thermal treatment temperature of 1300°C for 2 hours at a ramping rate of 5℃/min under an Argon environment in a high-temperature tube furnace (Carbolite Gero).

AHC-150°C: 7.5g of CG3 was weighed and pre-oxidized at 150°C in a muffle oven for 2 hours. The pre-oxidized CG3 was then carbonized at a thermal treatment temperature of 1300°C, for 2 hours at a ramping rate of 5℃/min under an Argon environment in a high-temperature tube furnace (Carbolite Gero).

AHC-600°C: 9.92g of CG3 was pre-pyrolyzed at a thermal treatment temperature of 600°C for 2 hours at a ramping rate of 5℃/min under an Argon environment in a high-temperature tube furnace. The resulting biochar was washed with deionized water for further removal of impurities and dried at 80°C for 12 hours. The dried biochar was then carbonized at a heat treatment temperature of 1300°C for 2 hours at a ramping rate of

$5℃/min$ under an Argon environment in a high-temperature tube furnace (Carbolite Gero).

AHC-1300°C: 7.0g of CG3 was directly carbonized at a thermal treatment temperature of 1300°C for 2 hours at a ramping rate of $5℃/min$ under an Argon environment in a high-temperature tube furnace (Carbolite Gero).

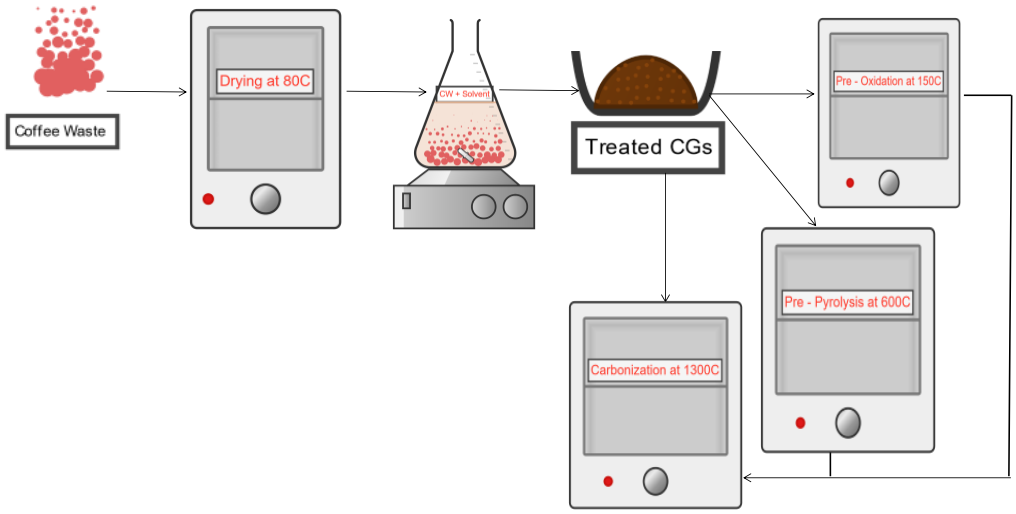

Figure 3.1.1. HC Synthesis from Coffee Waste employing different solvent treatment and Pre-treatment conditions.

3.2 Material Characterization

The structural properties of the synthesized HCs were analyzed employing electron microscopy techniques, Scanning Electron Microscopy (SEM) was used to study the HCs' morphological and surface structure, and Transmission Electron Microscopy (TEM) was used to determine the interparticle structure, orientation and interlayer spacings of the HCs. The graphene and defect bands of the HCs were studied using RAMAN Spectroscopy while X-ray Diffraction (XRD) analysis was used to evaluate the HCs' crystallinity and degree of graphitization.

3.3 Electrochemical Analysis

The electrodes were prepared using a mixing ratio of 8:1:1 of the synthesized CHCs, BHCs and AHCs (active material) : conductive material (Carbon Acetylene Black) : polymeric binder (polyvinylidene fluoride), all dissolved in NMP (N-methyl-2-pyrrolidone) and cast using the doctor blade technique on a copper current collector [26]. The slurry's solvents were removed by vacuum drying overnight at 60°C, a 14mm cutter was used to yield a 14mm electrode for the coincell. A Whatman paper served as a separator, soaked in 200 µL of electrolyte (consisting of 1 M NaPF6 EC: DMC: FEC).

Each component choice significantly impacts the electrochemical behavior. For instance, 1M NaPF6 dissolved in EC solvent improves capacity retention by forming a stable SEI layer. Simultaneously, the DMC solvent functions as a viscosity reducer, enhancing conductivity and allowing maximum enhancement in the low potential plateau. Cell assembly occurred within an argon environment glove box, ensuring water and oxygen content remained below 0.01 ppm.

Galvanostatic long term charge – discharge analysis of the assembled coin cells was carried out using a Neware Battery Testing System to investigate the electrochemical performance at a potential window between 0.01 and 2.50 V (vs. Na^+/Na) at a current density of $20mAg^{-1}$ [27], also employing different current density of $20mAg^{-1}$, $50mAg^{-1}$, $100mAg^{-1}$, and $200mAg^{-1}$ the influence of high capacity load supply on the stability and deliverable capacity of the assembled coin cells was studied.

Chapter 4 – Results and Discussion

4.1 Yield, Structural and Chemical Analysis of the Synthesized Hard Carbons

The sample preparation solvent shows a remarkable effect on the yield of the CGs after the solvent washing, with CG1 producing the highest yield of 88% followed by CG2 with 85.3% yield and CG3 with the lowest yield of 80.69%. This trend in yield shows the effect of the solvent on the removal of impurities and inorganic matter where the CG3 with the lowest yield shows removal of impurities and inorganic matter which directly influence the weight of the acid-washed CG compared to the use of organic solvent and de-ionized water.

Table 4.1.1 Yield of Synthesized HCs from different solvents and pre-treatment conditions before carbonization at 1300℃.

Samples	CG1			CG2			CG3		
	CHC 150℃	CHC 600℃	CHC 1300℃	BHC 150℃	BHC 600℃	BHC 1300℃	AHC 150℃	AHC 600℃	AHC 1300℃
Initial mass (g)	10.0142	10.00	10.013	10.0142	10.00	10.0016	7.5	9.92	7.0
Final mass (g)	2.201	2.141	2.204	2.303	2.149	2.45	1.66	2.4	1.76
Yield, %	22	21.4	22	23	21.49	24.5	22.11	24.19	25.14

Studying the yield of the synthesized HCs post carbonization, the directly carbonized CG (HC1300℃) shows the highest yield within the range of 22 – 25.2 % for all CGs samples regardless of the solvent used for the biowaste treatment, which is lower than the theoretically reported value of approximately 40 % yield post carbonization [16].

Also, HCs obtained through pre-oxidation pre-treatment conditions show approximately similar yield (22 – 23%) for all CG samples irrespective of the solvent used for the CG treatment as shown in Table 4.1.1

The morphological structures of the synthesized HCs were greatly influenced by the solvent used in the CG treatment as revealed in Figure 4.1.1 (a – i), The SEM images show the agglomeration of particles with varying porosity based on the solvent and pre-treatment conditions before carbonization.

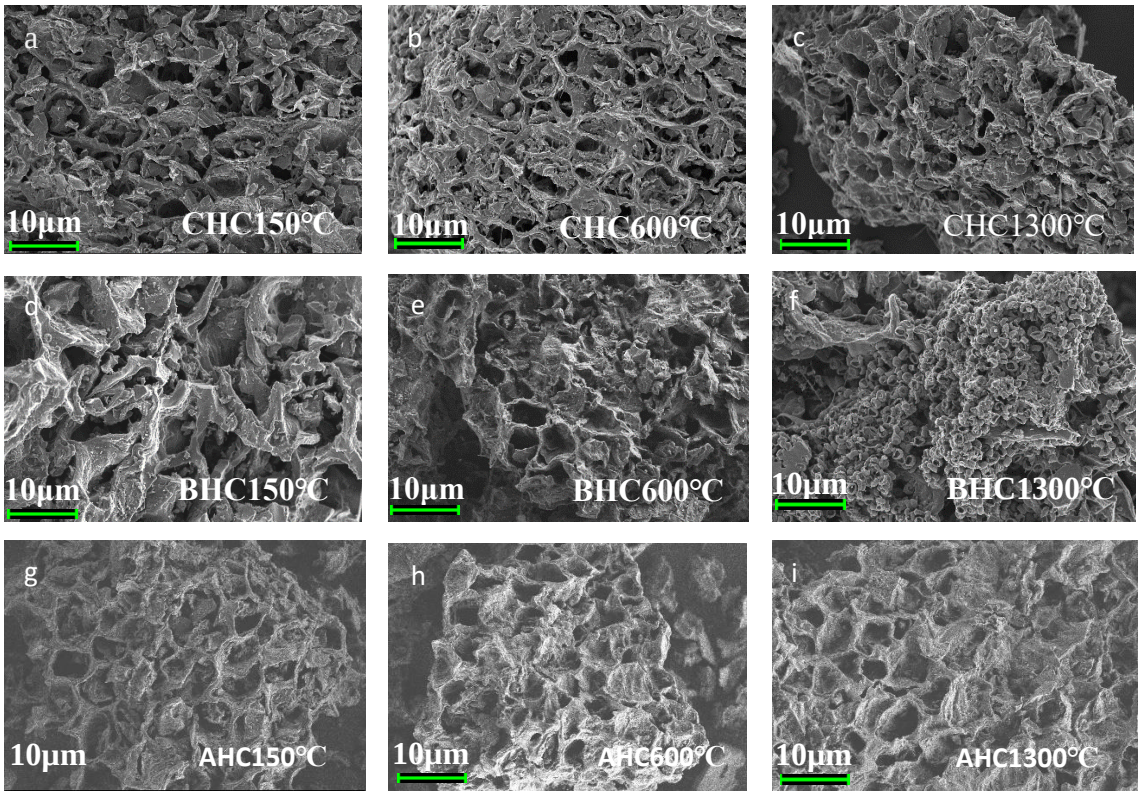

Figure 4.1.1: SEM images of Synthesized HCs from different solvents and pre-treatment conditions.

As shown in figure 4.1.1 a-c, the organic solvent used in the treatment of the CG1 majorly influenced the morphology of the resulting CHCs with more loose and porous structure compared to CG2 (d – f) with more compact morpholgy especially with the BHC1300°C with highly agglomerated cluster of small pores and CG3 (g – i) with highly porous honeycomb structure owing to signficant removal of inorganic matters and impurities due to acid treatment. SEM images of the pre – oxidized samples (a, d &g) show more internal

pores which may be due to the pre-oxidation treatment that increases oxygen content and favours sodium insertion [28], while the pre – pyrolysis treatment influenced the density in comparison to other pre-treatment condition used for same CG samples [29].

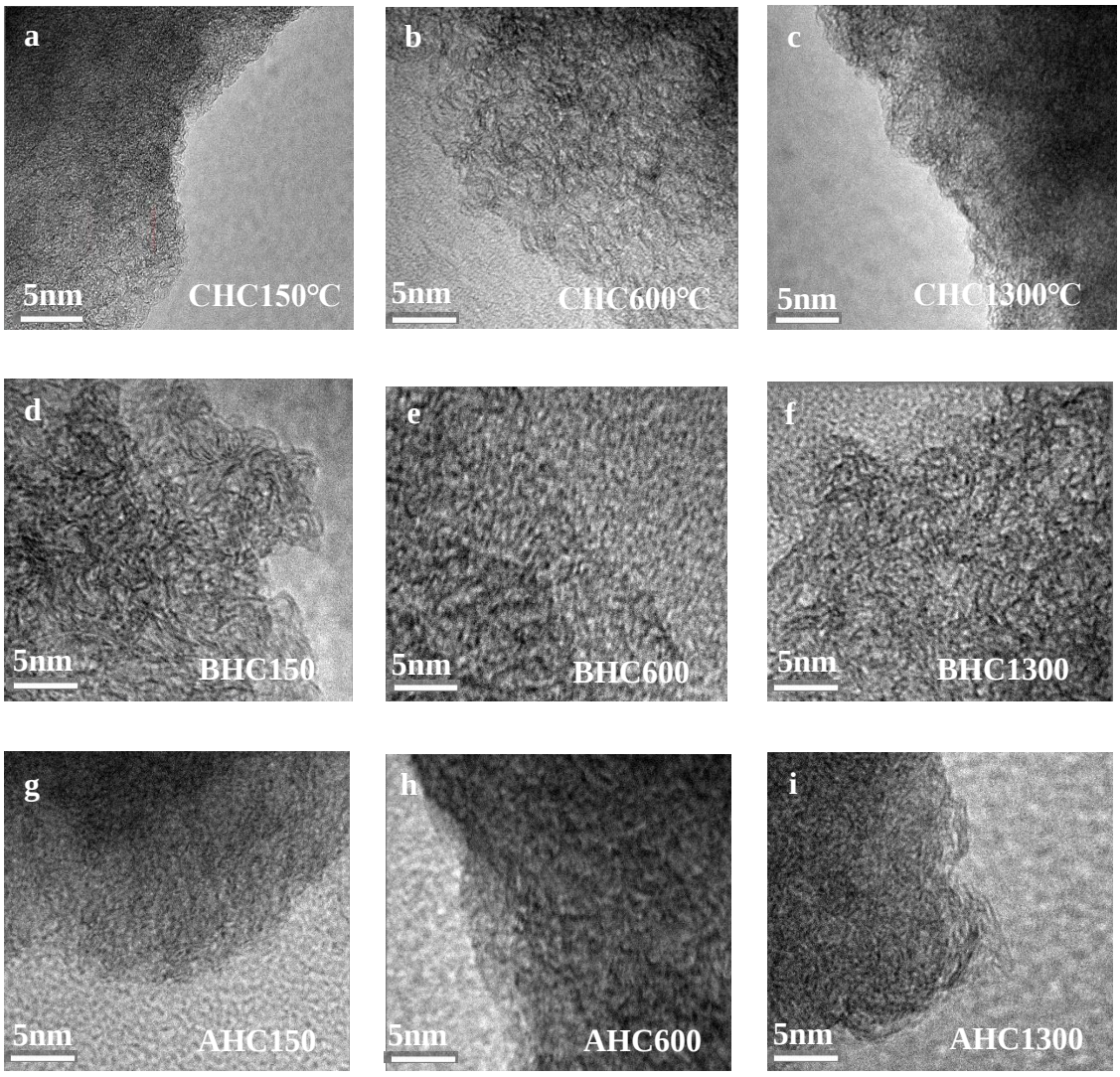

Figure 4.1.2: TEM images of Synthesized HCs from different solvents and pre-treatment conditions.

TEM images of the synthesized HCs as shown in Figure 4.1.2 revealed quite similar graphene layer stacking and disorderliness for all the samples regardless of the solvent and pre-treatment conditions, the results which are identical to the reported features of HC interparticle arrangement [25, 30]. The solvent and pre-treatment conditions played a major

role in enhancing the interlayer distance and disorderliness between the graphene layers as the synthesized HCs from organic solvent (Fig. 4.1.2 a – c) possessed larger interlayer spacing ranging from 0.437nm to 0.783 nm based on average d- spacing obtained from the FFT of the images which show the degree of separation between graphene layers.

Although the pre-oxidized samples demonstrated the lowest interlayer spacing between 0.438 – 0.372nm for all three solvents, with acid treated sample (AHC 150℃) having the lowest interlayer spacing of 0.372nm and De-ionized water treated sample (BHC 150℃) having an interlayer spacing of 0.378nm, irrespective of the pre-treatment solvent, direct thermal treatment at 1300℃ shows higher interlayer spacing for all the C. However ,all the synthesized HCs possess sufficient interlayer spacing for sodium ion insertion and extraction into the hard carbon structure (> 0.34nm) [23].

The synthesized HCs XRD diffractograms illustrated in Figure 4.1.3 (a – c) show the typical 002 and 100 broad peaks around 23° and 42° which is identical for all disordered carbon structures [26]. Employing the Peak Analyzer function of Origin software, the 002 peaks were fitted to deduce the peak angles used to calculate the graphitic interlayer distance (d_{002}), height (Lc), and number of graphene sheets in each layer (N). Using equation 4.1.1 – 4.1.3, where λ =0.154nm for the incident ray employed in XRD analysis.

$$d_{002} = \frac{\lambda}{2 \sin \theta_{002}} \qquad \text{eqn 4.1.1}$$

$$L_c = \frac{0.9\,\lambda}{\beta_{002} \cos \theta_{002}} \qquad \text{eqn 4.1.2}$$

$$\mathrm{N} = \frac{L_c}{d_{002}} \qquad \text{eqn 4.1.3}$$

pre-treatment conditions effect on the carbon structure is detected by the slight shift of the 002 peak to lesser angles compared to the 002 peak angle of direct thermally treated HCs except for the acid-washed sample. This shift in 002 peaks to the left directly increases the estimated interlayer spacing of the HCs, with the pre-oxidized HC demonstrating the lowest number of graphene sheets as reported in Table 4.1.2.

Table 4.1.2: XRD parameters of Synthesized HCs from different Solvents and pre–treatment conditions.

Sample	CG1			CG2			CG3		
	CHC 150℃	CHC 600℃	CHC 1300℃	BHC 150℃	BHC 600℃	BHC 1300℃	AHC 150℃	AHC 600℃	AHC 1300℃
2θ	23.57	23.54	23.611	23.49	23.396	24.086	23.119	23.361	22.93
θ	11.785	11.77	11.8055	11.745	11.698	12.043	11.559	11.681	11.465
d_{002}	0.377	0.377	0.376	0.378	0.38	0.369	0.384	0.38	0.387
L_c	2.02	2.08	2.07	2.02	2.06	2.41	1.89	2.08	1.97
N	5.4	5.5	5.5	5.3	5.4	6.5	4.9	5.5	5.1

Inferring from Table 4.1.3, the disordered carbon possessed comparable interlayer spacing which is attributed to the similar crystallization and graphitization degree owing to the same carbonization temperature for the synthesized HCs. However, the L_c and N values of the synthesized HCs ranged between 1.89 – 2.41 and 4.9 – 6.5, with BHC-1300℃ demonstrating the highest graphene stacking (N) and graphitic domain height (L_c), which is supported with its uniques SEM morphology and TEM image.

The Raman Spectra of the synthesized HCs show the disordered carbon characteristic Graphite and Defect bands detected around 1560 and 1360 cm^{-1} [23]. As illustrated in Figure 4.1.3 (d – f) the Raman Spectra provide additional information about the HCs structural arrangement, defects and graphitic domain thickness (L_a) implementing the intensity ratio $\left({}^{I_D}/_{I^G}\right)$ and equation 4.1.4

$$L_a = (2.4 \times 10^{-10})\, \lambda^4 \left(\frac{I_D}{I_G}\right)^{-1} \qquad \text{eqn 4.1.4}$$

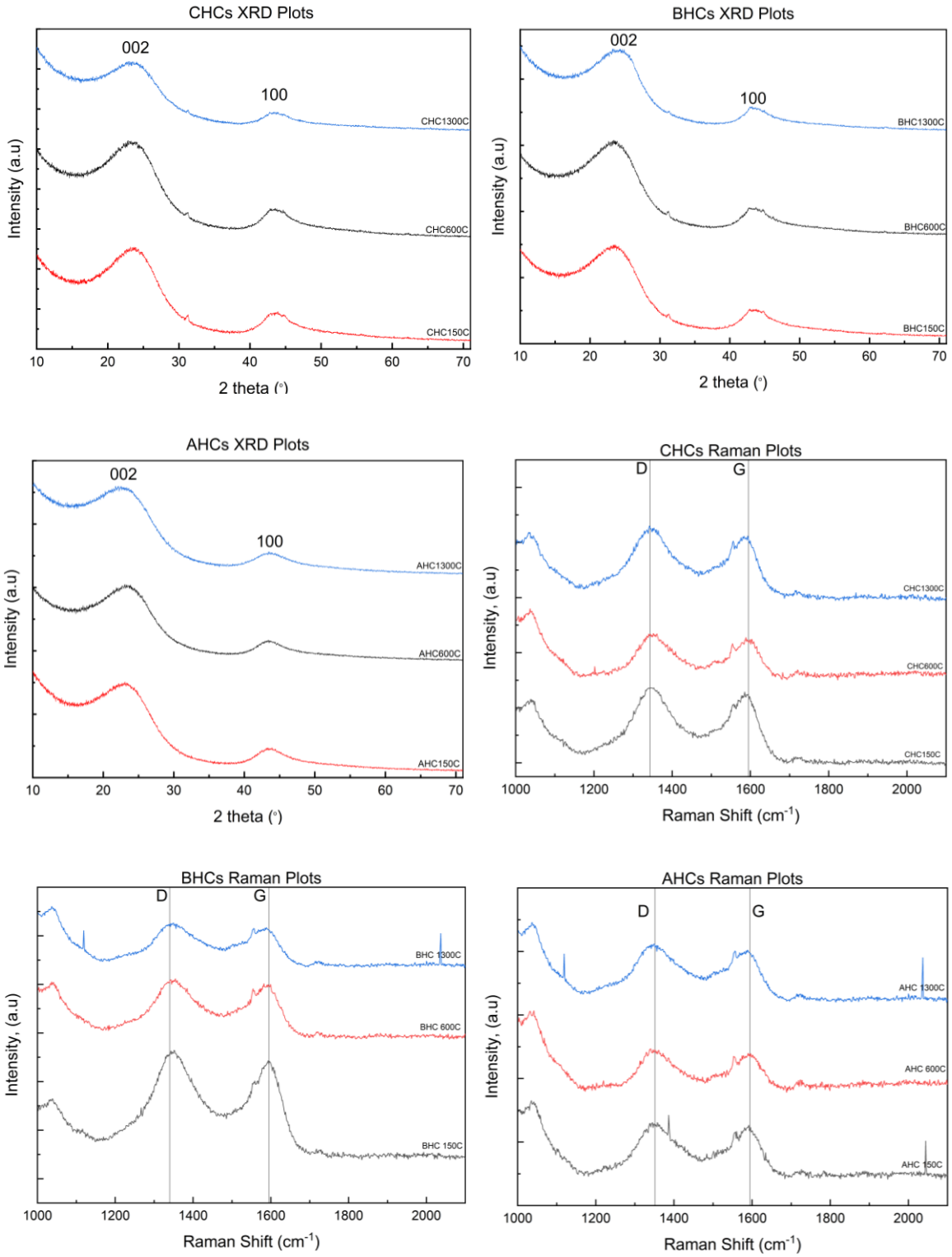

Figure 4.1.3: XRD and RAMAN Plots of Synthesized HCs from different solvents and Pre-treatment Conditions.

Table 4.1.4 Raman Parameters of Synthesized HCs from different Solvents and Pre – treatment Conditions.

Samples	CG1			CG2			CG3		
	CHC 150℃	CHC 600℃	CHC 1300℃	BHC 150℃	BHC 600℃	BHC 1300℃	AHC 150℃	AHC 600℃	AHC 1300℃
I_D	1364	1361	1364	1365	1366	1372	1373	1372	1375
I_G	1564	1577	1561	1574	1564	1564	1565	1571	1565
I_D / I_G	0.87	0.86	0.87	0.87	0.87	0.88	0.88	0.87	0.88
L_a	19.25	19.48	19.25	19.25	19.25	19.04	19.04	19.25	19.04

The deduced intensity ratio of the HCs are closely similar (0.87) this shows that the pre–treatment conditions and solvent type do not influence the defect sites, while the L_a values of the synthesized HCs are approximately the same (19nm), the values ranged from 19.04 – 19.48 with most of the structures demonstrating similar graphitic thickness of 19.25 with the exemption of CHC 600 ℃ demonstrating the largest width of 19.48nm and CHC 600℃, AHC 150℃ and 1300℃ showed the lowest width of 19.04nm as reported in Table 4.1.3.

4.2 Electrochemical Performance

The effect of washing solvent and pre-treatment conditions on the synthesized HCs electrochemical performance was investigated with the aid of the galvanostatic voltage profiles, the electrochemical profile of the HCs during the 1st and 2nd cycle demonstrated curves identical to the typical HC electrochemical behaviour, the thermal treatment temperature (1300℃) significantly contributes to the low capacity gain at the slope region as shown in Figure 4.2.1 (a– i) , as increase in the thermal treatment temperature decreases the edge and defect sites available for sodium ion adsorption [31], since the HCs are synthesized at the same temperature, the electrodes possess similar edge and defect sites for sodium insertion and extraction.

The Carbonization temperature (1300℃) provided the required interlayer distance for Na^+ intercalation into the HC pores by improving the graphene layers order and closed micropores for sodium storage which directly increased the capacity gain at the plateau region [32], Solid Electrolyte Interface (SEI) development after the 1st cycle is majorly responsible for the non-reversible capacity loss experienced post 1st cycle except in the case of AHC 600℃ and 1300℃ where the irreversible capacity was over 110$mAhg^{-1}$ as shown in Table 4.2.1. this large fall in capacity can be traced to significant sodium ion trapping as a result of more open pores and defects sites due to the washing solvent (acid) which increases the removal of impurities and favors the development of defect sites while increasing the electrode porosity [32, 33].

The pre-oxidized electrodes demonstrated highest deliverable capacity of 267, 304 & 281 mAg^{-1} with ICE of 77.6, 78.2 &75.4% for CHC-150℃, BHC-150℃ & AHC-150℃ respectively as reported in Table 4.2.1. This exceptional trend can be linked to pre-oxidation effect on the HC microstructure by decreasing the degree of graphitization owing to the structure reticulation as a result of increase in oxygen composition, increase in the degree of amorphization directly improves the bending of the graphitic domain which promotes the formation of closed micropores for clustered sodium ion intercalation which is responsible for the increase of the pre-oxidized HC deliverable capacity compared to other HCs synthesized from using same washing solvents [19, 29].

Although the pre-oxidized HC obtained from Deionized water treated CG delivered the highest specific discharge capacity of about 300 $mAhg^{-1}$, acid-washed HC exhibited the maximum reversible capacity of 262 and 265mAhg-1 for the pre-pyrolyzed and direct thermal treatment HCs. The lowest ICE for all synthesized HCs within the range of 75.4 – 64.6 % was reported for the acid-washed sample, This shows the effect of acid treatment on the HC structure post-carbonization, through the formation of more defect sites and open pores for sodium ion trapping which leads to decrease in ICE and reversible capacity even though the initial discharge capacities are higher due to increase surface area and removal of the positive effect of the inorganic impurities due to washing with acid [17].

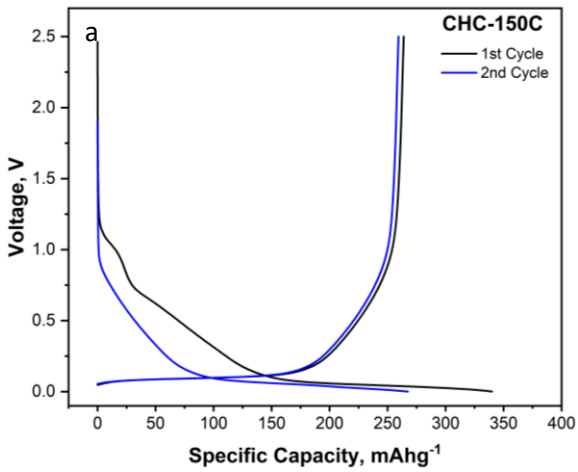
a
CHC-150C
1st Cycle
2nd Cycle
Voltage, V
Specific Capacity, mAhg-1

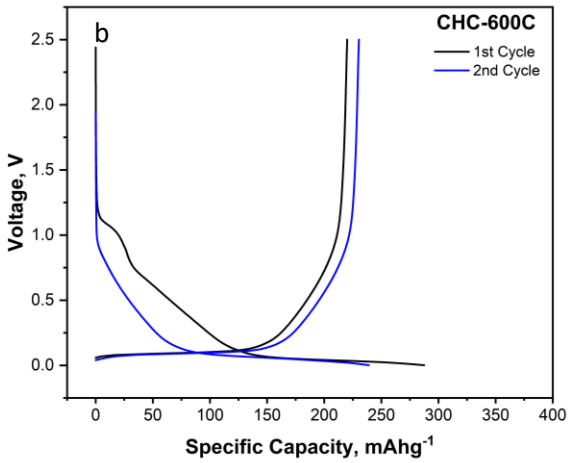
b
CHC-600C
1st Cycle
2nd Cycle
Voltage, V
Specific Capacity, mAhg-1

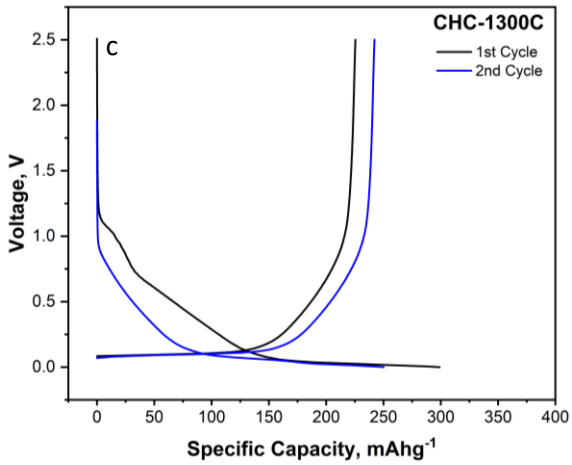
c
CHC-1300C
1st Cycle
2nd Cycle
Voltage, V
Specific Capacity, mAhg-1

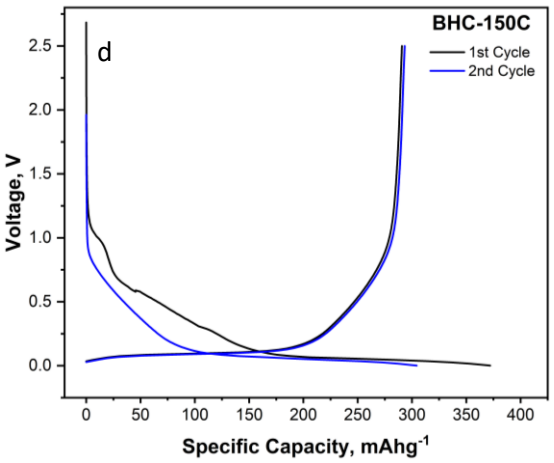
d
BHC-150C
1st Cycle
2nd Cycle
Voltage, V
Specific Capacity, mAhg-1

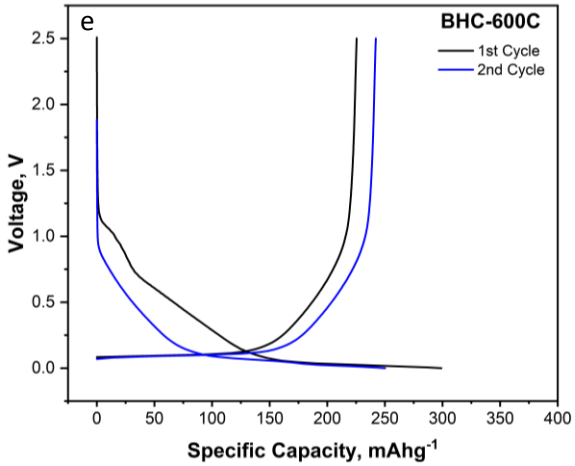
e
BHC-600C
1st Cycle
2nd Cycle
Voltage, V
Specific Capacity, mAhg-1

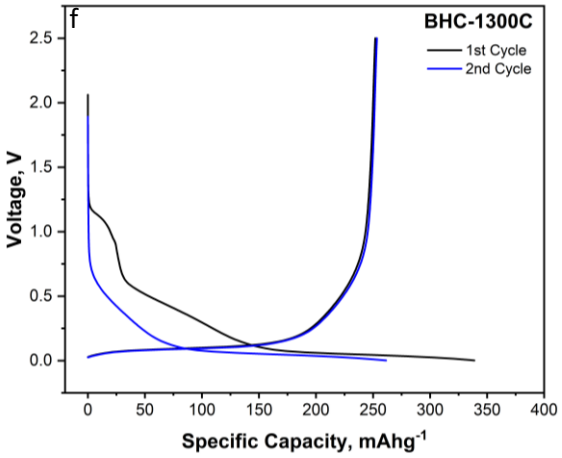
f
BHC-1300C
1st Cycle
2nd Cycle
Voltage, V
Specific Capacity, mAhg-1

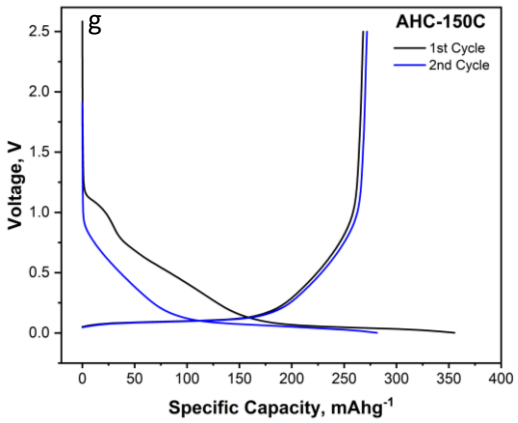
g
AHC-150C
1st Cycle
2nd Cycle
Voltage, V
Specific Capacity, mAhg-1

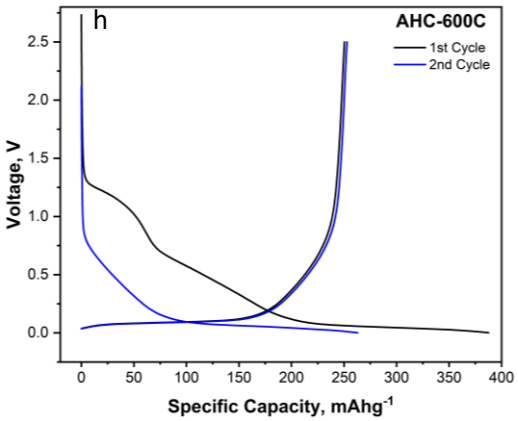
h
AHC-600C
1st Cycle
2nd Cycle
Voltage, V
Specific Capacity, mAhg-1

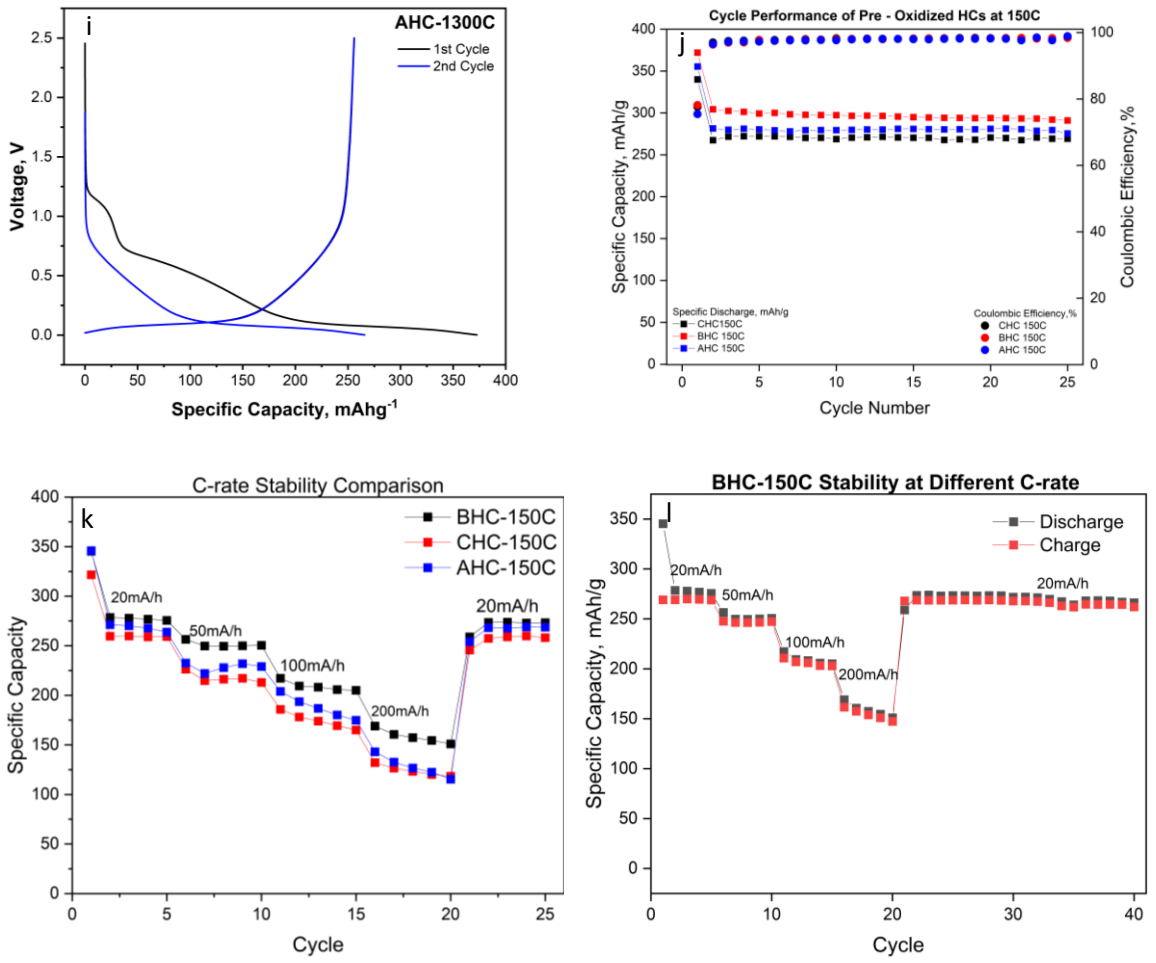

Figure 4.2.1 Galvanostatic Charge -Discharge Profile of Synthesized HCs Electrodes (a-i), Cycle Performance of Pre -Oxidized HCs 150℃ at a Current rate of 20mA/h (j) and Stability of the Pre – oxidized HCs at different current density (k&l).

Evaluating the capacity retention of the pre-oxidized HCs over long-term cycling, the pre-oxidized HCs demonstrated excellent cycling stability and capacity retention of over 80 % even after over 20 cycles by delivering stable cycling capacity of 269, 292 & 279 mAhg-1 for CHC-150℃, BHC-150℃ and AHC-150℃ respectively as illustrated in Figure 4.2.1 (j). However, BHC-150℃ unique electrochemical performance could be traced to its perfect interlayer spacing of 0.378 nm, loose morphology illustrated in Figure 4.1.1 (d) coupled with the positive effects of pre-oxidation and washing solvent that promotes the formation of curved graphene layers that favour closed micropores development and

presence of inorganic impurities which induce slight but favorable change on the HC microporous structure respectively.

Table 4.2.1: Electrochemical Performances of HCs from Different Solvent and Pre-treatment Conditions.

Samples	CG1			CG2			CG3		
	CHC 150 ℃	CHC 600 ℃	CHC 1300 ℃	BHC 150 ℃	BHC 600 ℃	BHC 1300 ℃	AHC 150 ℃	AHC 600 ℃	AHC 1300 ℃
1st Discharge, mAhg-1	340	287	299	372	299	339	356	387	373
1st Charge, mAhg-1	264	220	225.5	**291**	226	252	268	250	256
2nd Discharge, mAhg-1	267	239	250	**304**	250	261	281	262	265
2nd Charge, mAhg-1	259	230	242	**293**	242	253	272	252	256
Coulombic Efficiency, %	77.6	76.6	75.4	**78.2**	75.4	74.4	75.4	64.6	68.7
Irreversible Capacity, mAhg-1	76	67	73	81	73	87	88	137	117

Conclusion

The washing-solvent and pre-treatment conditions before the thermal treatment played a significant role in determining the hard-carbon yield, structure and electrochemical performance. The coffee-waste-derived HC demonstrated a yield within the range of 20 percent which is lower than the theoretically reported yield of hard carbon obtained from coffee-waste. The directly carbonized HC demonstrated the highest yield for all the CGs.

The pre-treatment conditions and washing solvents' effects on the morphological structure directly influence the porosity, interlayer distance and defect sites which consequentially determines the electrochemical behaviour. BHC-150℃ demonstrated the highest deliverable capacity (304 $mAhg^{-1}$) using a current density of 20 mAg^{-1} and excellent stability over different current density tests. This is attributed to its exceptional interlayer spacing, pore size distribution and defect sites which favor sodium ion insertion and extraction from the electrode with minimal loss owing to ions trapped in open pores and SEI formation.

Additionally, preoxidation at 150℃ for 2 hours lowers the degree of graphitization by increasing oxygen composition in the sample which favours the formation of curved graphene domains. The formation of curved domains is beneficial to the development of closed pores which are essential for clustered ion intercalation. The variation of the deliverable capacity of the pre-oxidized electrode demonstrated the intensity of the washing solvent on the degree of inorganic impurities present and defects sites formed in the CGs and HC structure post-carbonization. D.I. water showed the optimal removal of impurities and forming defect sites suitable for high-capacity electrodes for SIBs.

Conclusively, a combination of optimal sample preparation method (D.I as washing solvent), amorphization-enhancing pre-treatment condition (pre-oxidation at 150℃), optimal thermal treatment (carbonization at 1300℃) and use of suitable electrolytes enhances the capacity of coffee-waste-derived HC through the formation of a porous structure with enough interlayer spacing for ion insertion, minimal defect sites which increases capacity gain at the plateau region and stable SEI that reduces irreversible capacity loss.

References

[1] N. Sun, H. Liu, and B. J. J. o. m. c. a. Xu, "Facile synthesis of high performance hard carbon anode materials for sodium ion batteries," vol. 3, no. 41, pp. 20560-20566, 2015.

[2] J. B. Goodenough and K.-S. J. J. o. t. A. C. S. Park, "The Li-ion rechargeable battery: a perspective," vol. 135, no. 4, pp. 1167-1176, 2013.

[3] N. Yabuuchi, K. Kubota, M. Dahbi, and S. J. C. r. Komaba, "Research development on sodium-ion batteries," vol. 114, no. 23, pp. 11636-11682, 2014.

[4] K. Kubota and S. J. J. o. T. E. S. Komaba, "practical issues and future perspective for Na-ion batteries," vol. 162, no. 14, p. A2538, 2015.

[5] S. Alvin, H. S. Cahyadi, J. Hwang, W. Chang, S. K. Kwak, and J. J. A. E. M. Kim, "Revealing the intercalation mechanisms of lithium, sodium, and potassium in hard carbon," vol. 10, no. 20, p. 2000283, 2020.

[6] Y. Wen *et al.*, "Expanded graphite as superior anode for sodium-ion batteries," vol. 5, no. 1, p. 4033, 2014.

[7] I. T. Kim, E. Allcorn, and A. J. J. o. P. S. Manthiram, "Cu6Sn5–TiC–C nanocomposite anodes for high-performance sodium-ion batteries," vol. 281, pp. 11-17, 2015.

[8] D. Stevens and J. J. J. o. t. E. S. Dahn, "High capacity anode materials for rechargeable sodium-ion batteries," vol. 147, no. 4, p. 1271, 2000.

[9] D. Alvira, D. Antorán, and J. J. J. C. E. J. Manyà, "Plant-derived hard carbon as anode for sodium-ion batteries: A comprehensive review to guide interdisciplinary research," p. 137468, 2022.

[10] Y. Zheng *et al.*, "Superior electrochemical performance of sodium-ion full-cell using poplar wood derived hard carbon anode," *Energy Storage Materials,* vol. 18, pp. 269-279, 2019/03/01/ 2019.

[11] S. V. Vassilev, D. Baxter, L. K. Andersen, and C. G. Vassileva, "An overview of the chemical composition of biomass," *Fuel,* vol. 89, no. 5, pp. 913-933, 2010/05/01/ 2010.

[12] L. Yang, M. Hu, Q. Lv, H. Zhang, W. Yang, and R. Lv, "Salt and sugar derived high power carbon microspheres anode with excellent low-potential capacity," *Carbon,* vol. 163, pp. 288-296, 2020/08/15/ 2020.

[13] X.-S. Wu, X.-L. Dong, B.-Y. Wang, J.-L. Xia, and W.-C. J. R. E. Li, "Revealing the sodium storage behavior of biomass-derived hard carbon by using pure lignin and cellulose as model precursors," vol. 189, pp. 630-638, 2022.

[14] S. Alvin *et al.*, "Revealing sodium ion storage mechanism in hard carbon," vol. 145, pp. 67-81, 2019.

[15] X. Chen *et al.*, "An overall understanding of sodium storage behaviors in hard carbons by an “adsorption-intercalation/filling” hybrid mechanism," vol. 12, no. 24, p. 2200886, 2022.

[16] G. A. Figueroa Campos *et al.*, "Preparation of activated carbons from spent coffee grounds and coffee parchment and assessment of their adsorbent efficiency," vol. 9, no. 8, p. 1396, 2021.

[17] A. Beda, J.-M. Le Meins, P.-L. Taberna, P. Simon, C. M. J. S. M. Ghimbeu, and Technologies, "Impact of biomass inorganic impurities on hard carbon properties and performance in Na-ion batteries," vol. 26, p. e00227, 2020.

[18] P.-H. Chiang *et al.*, "Coffee-ground-derived nanoporous carbon anodes for sodium-ion batteries with high rate performance and cyclic stability," vol. 34, no. 6, pp. 7666-7675, 2020.

[19] N. Daher, D. Huo, C. Davoisne, P. Meunier, and R. l. J. A. A. E. M. Janot, "Impact of preoxidation treatments on performances of pitch-based hard carbons for sodium-ion batteries," vol. 3, no. 7, pp. 6501-6510, 2020.

[20] S. Guo, Y. Chen, L. Tong, Y. Cao, H. Jiao, and X. J. E. A. Qiu, "Biomass hard carbon of high initial coulombic efficiency for sodium-ion batteries: preparation and application," vol. 410, p. 140017, 2022.

[21] J. Ding *et al.*, "Sulfur and phosphorus co-doped hard carbon derived from oak seeds enabled reversible sodium spheres filling and plating for ultra-stable sodium storage," *Journal of Alloys and Compounds,* vol. 851, p. 156791, 2021/01/15/ 2021.

[22] Y. Liu, D. J. Lee, H.-J. Ahn, S. Y. Nam, K.-K. Cho, and J.-H. J. R. E. Ahn, "Waste coffee grounds-derived carbon: Nanoarchitectured pore-structure regulation for sustainable room-temperature sodium–sulfur batteries," vol. 212, pp. 865-874, 2023.

[23] H.-Y. Hu *et al.*, "A Stable Biomass-Derived Hard Carbon Anode for High-Performance Sodium-Ion Full Battery," vol. 9, no. 1, p. 2000730, 2021.

[24] L. Ma *et al.*, "The novel N-rich hard carbon nanofiber as high-performance electrode materials for sodium-ion batteries," *Ceramics International,* vol. 47, no. 7, Part A, pp. 9118-9124, 2021/04/01/ 2021.

[25] H. Wan *et al.*, "Biomass-derived N/S dual-doped porous hard-carbon as high-capacity anodes for lithium/sodium ions batteries," *Energy,* vol. 231, p. 121102, 2021/09/15/ 2021.

[26] K.-l. Hong *et al.*, "Biomass derived hard carbon used as a high performance anode material for sodium ion batteries," vol. 2, no. 32, pp. 12733-12738, 2014.

[27] G. Gao, L.-Z. Cheong, D. Wang, and C. J. C. R. C. Shen, "Pyrolytic carbon derived from spent coffee grounds as anode for sodium-ion batteries," vol. 1, no. 1, pp. 104-108, 2018.

[28] A. Kamiyama *et al.*, "MgO-Template Synthesis of Extremely High Capacity Hard Carbon for Na-Ion Battery," *Angewandte Chemie International Edition,* vol. 60, no. 10, pp. 5114-5120, 2021/03/01 2021.

[29] X. Lin, Y. Liu, H. Tan, and B. Zhang, "Advanced lignin-derived hard carbon for Na-ion batteries and a comparison with Li and K ion storage," *Carbon,* vol. 157, pp. 316-323, 2020/02/01/ 2020.

[30] S. J. Hong, S. S. Kim, S. J. C. S. Nam, and Technology, "Using coffee-derived hard carbon as a cost-effective and eco-friendly anode material for li-ion batteries," vol. 20, no. 1, pp. 15-21, 2021.

[31] P. Liu, Y. Li, Y.-S. Hu, H. Li, L. Chen, and X. J. J. o. M. C. A. Huang, "A waste biomass derived hard carbon as a high-performance anode material for sodium-ion batteries," vol. 4, no. 34, pp. 13046-13052, 2016.

[32] L. Xiao *et al.*, "Low-defect and low-porosity hard carbon with high coulombic efficiency and high capacity for practical sodium ion battery anode," vol. 8, no. 20, p. 1703238, 2018.

[33] A. Kamiyama *et al.*, "MgO-Template Synthesis of Extremely High Capacity Hard Carbon for Na-Ion Battery," vol. 60, no. 10, pp. 5114-5120, 2021.

Appendix A

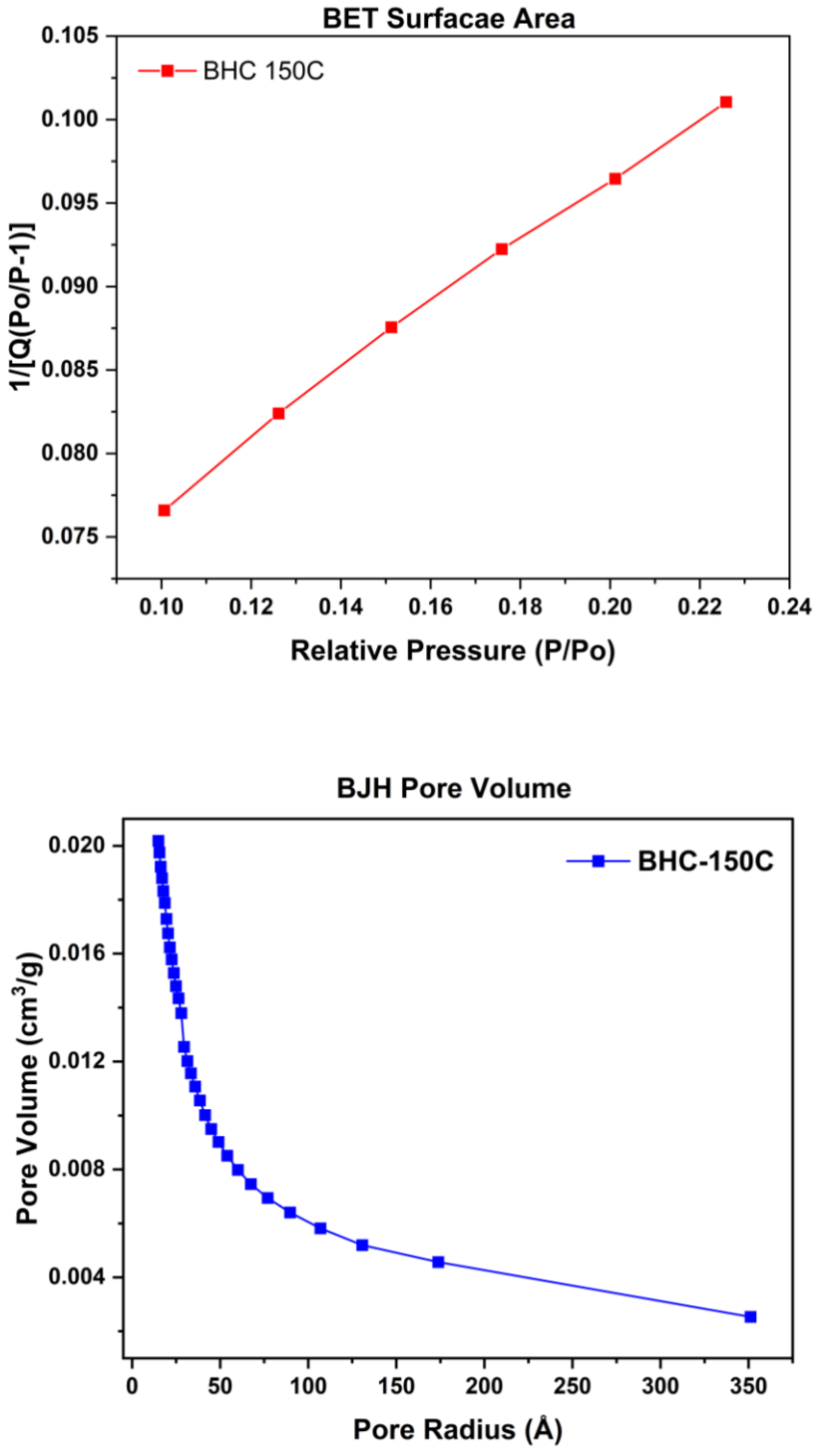

Figure A. BET Surface area and Pore Volume Plot of BHC-150C.